Korean J. Chem. Eng., 34(1), 87-99 (2017)
DOI: 10.1007/s11814-016-0242-z

pISSN: 0256-1115
eISSN: 1975-7220

Enhancement of gasoline selectivity in combined reactor system consisting of steam reforming of methane and Fischer-Tropsch synthesis

Abbas Ghareghashi*, Farhad Shahraki*,†, Kiyanoosh Razzaghi*, Sattar Ghader, and Mohammad Ali Torangi*****

*Department of Chemical Engineering, University of Sistan and Baluchestan, Zahedan 98164-161, Iran
**Department of Chemical Engineering, College of Engineering, Shahid Bahonar University of Kerman, Kerman, Iran
***Faculty of Engineering, University of Golestan, Gorgan, Iran
(*Received 24 June 2016 • accepted 23 August 2016*)

Abstract−A two-stage, one-dimensional configuration model including the steam reforming of methane (SRM) and Fischer-Tropsch (FT) synthesis has been developed for the production of hydrocarbons. This configuration is used to investigate hydrocarbon product distribution, such as gasoline. The first SRM reactor is fed by methane and steam, and the products are converted to hydrocarbons by the second FT reactor. The model was solved numerically by applying the finite difference approximation, and the set of first-order ODEs was solved in the axial direction. The results show that complete conversion of hydrogen in the second reactor can be achieved although a small amount of carbon monoxide remains. Furthermore, at higher H_2O/CH_4 ratio (and low CO in feed), lower C_2-C_5 yield and selectivity is obtained.

Keywords: Steam Reforming of Methane, Fischer Tropsch, C_5 Yield, Consecutive Reactors, C_5 Selectivity, CO_2 Yield

INTRODUCTION

Gasoline is one of the most valuable hydrocarbons with demand for it increasing continuously. Currently, crude oil is the generation source of this valuable feed, but due to the decline of fossil energy sources, researchers are thinking about replacing crude oil with another raw material. Methane constitutes highest percentage of natural gas and contained in remote reserves in the world can be widely considered as an alternative to crude oil. Given that methane is a very large source that is less used in industry, conversion of methane to valuable hydrocarbons such as gasoline is a key stage for its use. The first step to convert methane into valuable hydrocarbons is to convert methane into synthesis gas. There are numerous ways to produce synthesis gas; however, the most common and economical process of synthesis gas production from methane in industrial scale is steam reforming of methane (SRM) [1]. Synthesis gas is an intermediate that holds many valuable uses. Once we have synthesis gas we have optionality, because synthesis gas has the building blocks to create all the products and chemicals currently generated in the petrochemical industry, such as methanol, hydrogen, ammonia, acetic acid and MTBE. Production of synthesis gas has provided efficient production of other chemicals, environmental benefits and a fuel source. As research continues and reactor configurations are improved, synthesis gas may become a source of fuels. However, the product of an SRM reactor can be used as feed of FT reactor by converting synthesis gas to valuable hydrocarbons. Numerous studies are carried out on the modeling of SRM reactor and improving its performance. Modeling of industrial SRM reactor by Soliman et al. [2] is one of the best researches on reforming reactors. To ensure high accuracy, they considered diffusion resistance in the modeling of catalyst particles. The effects of various parameters were also examined on reactor performance. Results indicated a very good agreement with various industrial reforming data. Mathematical model analysis by Adris et al. [3] showed that using a hydrogen permeable membrane increases the methane conversion.

De Falco et al. [4] studied the variations in both radial and axial directions for the more accurate simulation of reforming reactor in large scale. They compared the modeling results with conventional and membrane reactors. Sadooghi and Rauch [5] investigated a two-dimensional heterogeneous model for fixed bed SRM reactor by including temperature and pressure distribution terms in two axial and radial directions. The authors also investigated the effect of temperature variations on the reactor performance. They found that an increase of hydrogen yield can be achieved by increasing reactor temperature up to 1073 Wu et al. [6] proposed a method to increase the methane conversion in a catalytic fixed bed SRM reactor. They investigated the simultaneous effects of two factors for hydrogen separation by membrane as well as catalytic absorption of carbon dioxide on reactor performance. They found that both factors have a positive effect on methane conversion; however, the hydrogen separation factor has more effect.

In the second step, synthesis gas should be converted to valuable hydrocarbons. One of the key processes for converting synthesis gas to high value products is Fischer-Tropsch synthesis. This process is a complicated heterogeneous reaction that convert carbon monoxide and hydrogen on the surface of suitable catalyst to a mixture of hydrocarbons containing paraffins, olefins, oxygenated compounds, carbon dioxide and steam. Various types of reactors, including fixed bed, fluidized and slurry reactor, have been considered during the FTS process development for modern commercial applications. Originally, fixed bed reactors, in the form of

†To whom correspondence should be addressed.
E-mail: fshahraki@eng.usb.ac.ir

multi-tubular fixed bed reactors, were used for light temperature Fischer-Tropsch synthesis operations. The multi-tubular fixed bed Fischer-Tropsch process, being the one of the most competing reactor technologies, occupies a special position in FTS industrial practices, as shown by the large scale commercial operations of Sasol in South Africa and Shell in Malaysia. In these cases, the FT reaction takes place over an iron-based catalyst (Sasol) or over a cobalt-based catalyst (Shell) in a reactor that resembles a tubular heat exchanger with the catalyst packed in the tubes that are still used by Sasol in their Arge process and by Shell in the Shell Middle Distillate Synthesis process.

Considering the long history of FT synthesis, extensive research has been done in this field, particularly on the modeling of reactor. The pioneering work of Deckwer and Serpemen [7] is one of the first modeling on this subject. A one-dimensional heterogeneous model was employed in studying the FT reactor in large scale slurry phase. Simulation results showed that the two phenomena of catalyst settling and as solid-liquid mass transfer had negligible effect on reactor computations in large scale. Turner and Mills [8] studied FT synthesis in a slurry bubble column reactor. They applied each of the axial dispersion and mixing cell models to the simulation of reactor and compared the results of the two modes. They found better contact between gas and liquid in the co-current mode compared to counter-current mode and achieved better synthesis gas conversion in this case. Song et al. [9] presented mathematical modeling for slurry bed FT reactor. They investigated the variation of all process parameters to obtain favorable operating conditions. It has been shown that reducing the feed mass flux that could increase the conversions of CO and H2 more than 90% is most impressive method for improving both operability and performance of the FT reactor. They also reported that temperature variation had no significant effect on conversion and selectivity.

Wu et al. [10] investigated a pseudo-homogeneous model to simulate FT reactor and assumed that reactions just performed in external surface of catalyst pellet and internal part of catalyst were inactive. It was discovered that increase of pressure, unlike temperature and gas feed flow, has a significant effect on heavy hydrocarbons as well as synthesis gas conversion. Park et al. [11] examined the effect of tube diameter on reactor performance using a two-dimensional model. It was shown that increasing tube diameter is the factor greatly influencing the reactor temperature due to the exothermic nature of the reactions. Moreover, this increase in diameter improves the CO conversion as well as gasoline yield. In all of the work done so far, synthesis gas is fed to FT reactor in the form of prepared feed and specified H_2/CO ratio; however, it is attractive to use product of other processes as feedstock.

The process to produce valuable hydrocarbons from methane can be divided into two separate steps: syngas generation and syngas conversion. Although all of these technologies are well established, individually optimized and commercially proven, the combined use is not widely applied. However, to make this configuration more feasible, the challenge goes beyond the condition of known aspects of individual processes. It also includes those aspects that should be investigated and more importantly the effect of feed of SRM reactor on hydrocarbon synthesis in FTS.

Kim et al. [12] used an Aspen HYSYS simulation for gas-to-liquid process optimization. Auto-thermal reforming in synthesis gas production unit and slurry phase reaction over Co-based catalyst in FTS unit were considered as reaction models for the process. The effect of reaction temperature on CO conversion and C_5-C_{20} hydrocarbon yield in FTS unit was mainly examined. Simulation and experimental results showed that the optimum reaction temperature in the FTS unit was 255 °C.

Hydrogen production by consecutive reactor systems containing oxidative coupling and steam reforming of methane was developed by Avci et al. [13]. They applied the one-dimensional heterogeneous model for this mathematical investigation. They found that maximum hydrogen production achieved in lower amount of CH_4/O_2 ratio and higher H_2O/CH_4 ratio. Performance of the combining reactions of SRM and FT was experimentally investigated by Johns et al. [14] who studied the operation of a single catalyst at an intermediate temperature to combine these processes. To investigate the performance of the combined reactions, the kinetics of two different catalysts, Ru and Co, was applied in this study. The simulation results showed that low conversion of CH_4 could be obtained and catalysts with enhanced activity are required to attain more realistic conversions.

This paper addresses mathematical modeling of two consecutive SRM and FT reactors. A two-stage, one-dimensional, heterogeneous mathematical model has been developed to describe the reaction performance in both reactors. The model utilizes direct conversion of methane to hydrocarbons. Effects of reaction conditions as well as operating parameters on the products yield and selectivity are also investigated.

PROCESS DESCRIPTION AND MATHEMATICAL FORMULATION

Fig. 1 shows the schematic of the SRM and FT reactors. In this configuration, the first reactor is SRM and the second one is a conventional FT reactor. The reactants (methane, steam and nitrogen as diluents) are compressed up to 29 bar and heated to 793.15 K and then enter the SRM reactor where reforming reaction occurs. As soon as the SRM reactor is fed by reactant gases, mass transfer occurs on the surface of the catalyst particles. In addition, heat transfer also occurs between the walls and gases as well as between the gas and solid phases. SRM reactor is a fixed bed reactor which is packed with $Ni/MgAl_2O_4$ catalyst. The operational conditions of SRM reactor are listed in Table 1. The second reactor (FT reactor) is fed by the products of SRM reactor, including synthesis gas. Synthesis gas containing a mixture of CO and H2 enters the fixed bed FT reactor which is packed with Fe-HZSM5 catalyst. Then the synthesis gas is converted to valuable hydrocarbons. Table 2 indicates the characteristics of the FT reactor reported by RIPI [15]. A heat exchanger is placed between the two reactors to decrease SRM product temperature to FT feed temperature.

The Fe-HZSM5 catalyst is a physical mixture of an iron catalyst with a weight composition of metal part: 100Fe/5.4 Cu/7K_2O/21SiO_2 and an H-ZSM-5 zeolite. The preparation of catalyst is given in [16] as follows: first, HZSM-5 zeolite with SiO_2/Al_2O_3 ratio of 28 (BET surface area and pore volume were 313 m^2/g and 0.16 cm^3/g, respectively) was prepared. Both dried zeolite (80 wt%) and iron

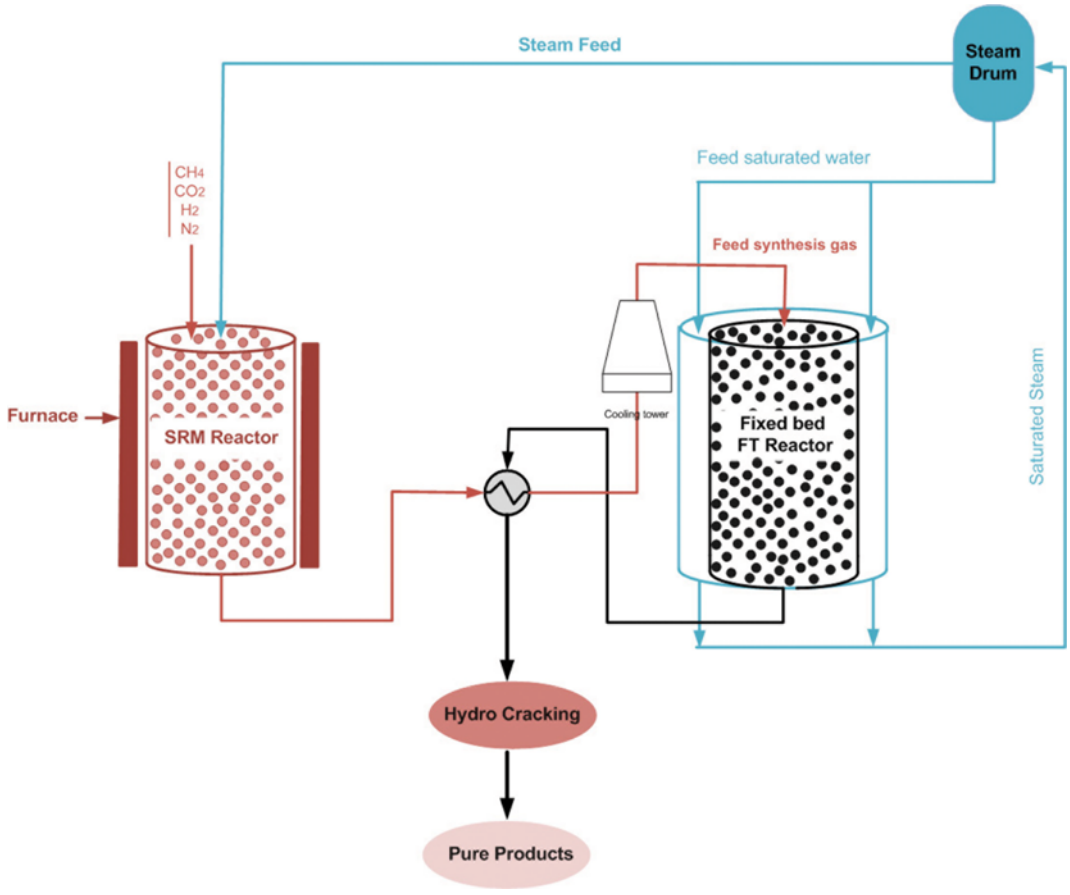

Fig. 1. Scheme of consecutive reactors: SRM and conventional FT synthesis reactor.

Table 1. SRM reactor characteristics [17]

Parameter	Value	Unit
Internal tube diameter	0.1016	m
External tube diameter	0.1322	m
Tube length	12	m
Heated tube length	11.12	m
Catalyst ring dimensions		
d_{pe}	0.0173	m
d_{pi}	0.0084	m
H	0.010	m
ρ_s	2355.2	kg/m^3
Thickness of active layer	0.002	m
Feed temperature	793.15	K
Feed inlet pressure	29	bar
CH_4 mole flow	5.168	kmol/hr
H_2O/CH_4 molar ratio	3.358	
CO_2/CH_4 molar ratio	0.056	
H_2/CH_4 molar ratio	0.122	
N_2/CH_4 molar ratio	0.164	

Table 2. RIPI FT Reactor characteristics [15]

Parameter	Value	Unit
Feed temperature	569	K
Cooling temperature	566.2	K
Tube dimension	Ø38.1×3×12,000	mm
Reactor pressure	1700	kPa
Catalyst sizes	Ø 2.51×5.2	mm
Catalyst density	1290	kg/m^3
Tube length	12	m
Number of tubes	1	
GHSV	235	1/hr
Bed voidage	0.488	
Feed molar flow rate	0.0335	gmol/s
Bulk density	730	kg/m^3

catalyst (20 wt%) were sieved to 60-mesh and mixed completely. Iron-zeolite catalyst was agglomerated with silica alumina solution (15 wt% of the total catalyst). The resulted paste-like gel was dried at 110 °C on perforated aluminum plate under reduced pressure to form 4 mm diameter and 3 mm high cylinders using a pelleting press. The catalyst cylinders were dried at 120 °C and then calcined at 450 °C in air and sieved to retain 250-300 μm.

1. Reactions Kinetics

1-1. SRM Model

The intrinsic kinetic expressions of methane steam reforming and water gas shift (WGS) reaction over $Ni/MgAl_2O_4$ catalyst have

been reported by Xu and Froment [17]. The main reaction scheme taken into account in SRM modeling are two catalytic reforming reactions, Eqs. (1) and (3), and the WGS reaction (Eq. (2)) that is rather exothermic.

$$CH_4+H_2O \rightleftharpoons CO+3H_2 \qquad \Delta H^0_{298}=+206\ \text{kJ/mol} \tag{1}$$

$$CO+H_2O \rightleftharpoons CO_2+H_2 \qquad \Delta H^0_{298}=-41\ \text{kJ/mol} \tag{2}$$

$$CH_4+2H_2O \rightleftharpoons CO_2+4H_2 \qquad \Delta H^0_{298}=+165\ \text{kJ/mol} \tag{3}$$

The relevant reactions rate equations are represented as follows:

$$R_1=\frac{\frac{k_1}{p_{H_2}^{2.5}}\left[p_{CH_4}p_{H_2O}-\frac{p_{H_2}^3 p_{CO}}{K_1}\right]}{DEN^2} \tag{4}$$

$$R_2=\frac{\frac{k_2}{p_{H_2}}\left[p_{CO}p_{H_2O}-\frac{p_{H_2}p_{CO_2}}{K_2}\right]}{DEN^2} \tag{5}$$

$$R_3=\frac{\frac{k_3}{p_{H_2}^{3.5}}\left[p_{CH_4}p_{H_2O}^2-\frac{p_{H_2}^4 p_{CO_2}}{K_3}\right]}{DEN^2} \tag{6}$$

$$DEN=1+K_{CH_4}p_{CH_4}+K_{CO}p_{CO}+K_{H_2}p_{H_2}+\frac{K_{H_2O}p_{H_2O}}{p_{H_2}} \tag{7}$$

where R_1, R_2 and R_3 are the rate equations of reactions (1), (2) and (3), respectively; k_1, k_2 and k_3 are rate coefficients of reactions; K_1, K_2 and K_3 the equilibrium constants of reactions; K_{CH_4}, K_{CO}, K_{H_2} and K_{H_2O} the adsorption coefficient constants of each component, and P_i is the partial pressure of the component i. The kinetic parameters of the above reaction rates are given in Table 3.

1-2. FT Model

A number of kinetic studies for FT synthesis are defined by the following reactions over Fe-HZSM5 catalyst that is given by Marvast et al. [15]. Reaction steps 1 to 8 are the recommended reactions to describe pilot plant (fixed-bed iron-based reactor) that produce a wide range of paraffins and olefins.

$$\text{Step 1: } CO+3H_2 \xrightarrow{R_1} CH_4+H_2O \tag{8}$$

$$\text{Step 2: } 2CO+4H_2 \xrightarrow{R_2} C_2H_4+2H_2O \tag{9}$$

$$\text{Step 3: } 2CO+5H_2 \xrightarrow{R_3} C_2H_6+2H_2O \tag{10}$$

$$\text{Step 4: } 3CO+7H_2 \xrightarrow{R_4} C_3H_8+3H_2O \tag{11}$$

$$\text{Step 5: } 4CO+9H_2 \xrightarrow{R_5} n\text{-}C_4H_{10}+4H_2O \tag{12}$$

$$\text{Step 6: } 4CO+9H_2 \xrightarrow{R_6} i\text{-}C_4H_{10}+4H_2O \tag{13}$$

$$\text{Step 7: } 6.05CO+12.23H_2 \xrightarrow{R_7} C_{6.05}H_{12.36}(C_5^+)+6.05H_2O \tag{14}$$

$$\text{Step 8: } CO+H_2O \xleftrightarrow{R_8} CO_2+H_2 \tag{15}$$

The general form of the reaction rate equation is expressed in terms of partial pressure of feed components as [18]:

$$R_i=0.278K_i\exp\left(\frac{-E_i}{RT}\right)P_{CO}^m P_{H_2}^n \tag{16}$$

where K_i is the pre-exponential factor, E_i the activation energy, R the gas universal constant and P_{CO} and P_{H_2} are the partial pressure of carbon monoxide and hydrogen, respectively. The kinetic parameters of each reaction are listed in Table 4.

2. Reactors Modeling

2-1. SRM Reactor Model

2-1-1. Gas Phase

The continuity equations for CH_4 and CO_2 components are as follows:

$$\frac{dX_{CH_4}}{dz}=\frac{\Omega\rho_B\eta_{CH_4}r_{CH_4}}{F^0_{CH_4}} \tag{17}$$

$$\frac{dX_{CO_2}}{dz}=\frac{\Omega\rho_B\eta_{CO_2}r_{CO_2}}{F^0_{CH_4}} \tag{18}$$

where X_i and z are conversion of components and length of reactor, respectively. Ω is the Cross section of the reactor, ρ_B the catalytic bed density, η_{CH_4} the effectiveness factor for methane disappearance, η_{CO_2} the effectiveness factor for CO_2 formation, r_{CH_4} the total rate of disappearance of CH_4 in steam reforming, r_{CO_2} the rate of conversion of CH_4 into CO_2 in steam reforming and F_i^0 is the molar flow rate of each component in the feed. The energy equa-

Table 3. Kinetic parameters of steam reforming of methane [17]

$k_i=A(k_i)\exp[-E_i/(RT)]$	for i=1, 2, 3	
$K_i=A(K_i)\exp[-\Delta H_i/(RT)]$	for i=1, 2, 3	
$K_j=A(k_j)\exp[-\Delta H_j/(RT)]$	for j=CH_4, H_2O, CO, H_2	
Activation energies (E kJ/mol)	Enthalpies change of reaction (ΔH kJ/mol)	
E_1=240.1	ΔH_1=206.1	ΔH_{CO}=−70.65
E_2=67.13	ΔH_2=−41.15	ΔH_{H_2}=−82.90
E_3=243.9	ΔH_3=164.9	ΔH_{CH_4}=−38.28
	ΔH_{H_2O}=88.68	
Pre-exponential terms		
$A(k_1)=4.225\times10^{15}$ (kmol·bar$^{1/2}$·kg^{-1}·h^{-1})		
$A(k_2)=1.955\times10^{6}$ (kmol·bar^{-1}·kg^{-1})		
$A(k_3)=1.02\times10^{15}$ (kmol·bar$^{1/2}$·kg^{-1}·h^{-1})		
$A(K_1)=4.707\times10^{12}$ (bar^2)		
$A(K_2)=1.142\times10^{-2}$		
$A(K_3)=5.375\times10^{10}$ (bar^2)		
$A(K_{CO})=8.23\times10^{-5}$ (bar^{-1})		
$A(K_{H_2})=6.12\times10^{-9}$		
$A(K_{CH_4})=6.65\times10^{-4}$ (bar^{-1})		
$A(K_{H_2O})=1.77\times10^{5}$ (bar^{-1})		

Table 4. Kinetic parameters of Fischer Tropsch synthesis [15]

Reaction no.	m	n	K_i	E_i
1	−1.0889	1.5662	142583.8	83423.9
2	0.7622	0.0728	51.556	65018
3	−0.5645	1.3155	24.717	49782
4	0.4051	0.6635	0.4632	34885.5
5	0.4728	1.1389	0.00474	27728.9
6	0.8204	0.5026	0.00832	25730.1
7	0.5850	0.5982	0.02316	23564.3
8	0.5742	0.710	410.667	58826.3

tion for gas phase is written as follows:

$$\frac{dT}{dz}=\frac{1}{c_p\rho_g u_s}\left[\rho_B\sum(-\Delta H_i)r_i\eta_i-4\frac{U}{d_{ti}}(T-T_r)\right] \quad (19)$$

where T is the process gas temperature, c_p the specific heat, ρ_g the density of system gas, u_s the superficial velocity, ρ_B the density of catalyst in the bed, ΔH_i the enthalpy change of reaction i, r_i the reaction rate of component i, η_i the effectiveness factor of reaction i for each reaction, U the overall heat transfer coefficient, d_{ti} the inner diameter of the reactor tube and T_r is the tube wall temperature. The momentum balance for gas phase is:

$$-\frac{dp_t}{dz}=\frac{f\rho_g u_s^2}{gd_p} \quad (20)$$

where p_t is total pressure of gas phase, u_s the superficial velocity and ρ_g the density of system gas. The equivalent diameter d_p is computed using the relation provided by Brauer [19]. The porosity of the bed ε is estimated using the equation obtained by Reichelt and Blasz [20] and f is calculated by using Ergun equation as follows [21]:

$$f=\frac{1-\varepsilon}{\varepsilon}\frac{1.74+150(1-\varepsilon)}{Re_{dp}} \quad (21)$$

The boundary conditions at z=0 are written as:

$$x_{CH_4}=x_{CO_2};\ T=T_0;\ p_t=p_{t_0}$$

The heat transfer coefficient is calculated using following correlation [22]:

$$\frac{1}{U}=\frac{d_{ti}}{2\lambda_{st}}\ln\left(\frac{d_{te}}{d_{ti}}\right)+\frac{1}{\alpha_i} \quad (22)$$

where d_{ti} and d_{te} are the inner and external diameters of the reactor tube, respectively; α_i is convective heat transfer coefficient in packed bed that expressed as follows [23]:

$$\alpha_i=\frac{8\lambda_{er}\alpha_w}{8\lambda_{er}+\alpha_w d_{ti}} \quad (23)$$

where

$$\alpha_w=\alpha_w^0+0.444RePr\frac{\lambda_g}{d_p} \quad (24)$$

$$\lambda_{er}=\lambda_{er}^0+0.14\lambda_g RePr \quad (25)$$

where λ_g is the thermal conductivity of the process gas. α_w^0 is given by [21]:

$$\alpha_w^0=\frac{8.694}{(d_{ti})^{4/3}}\lambda_{er}^0 \quad (26)$$

where λ_{er}^0 obtained from relation presented by Kunii and Smith [24].

2-1-2. Solid Phase

The following equation is used to obtain the concentration gradients of CH_4 and CO_2 components inside the catalyst particle:

$$\frac{1}{\xi^2}\frac{d}{d\xi}\left(D_{e,i}\xi^2\frac{dp_{s,i}}{d\xi}\right)=10^{-2}RT\cdot R_p^2\cdot r_i'\cdot p_s\cdot\rho_s \qquad i=CH_4, CO_2 \quad (27)$$

where ξ is the radial position in particle, R the universal gas constant, R_p the equivalent radius of the catalyst particle and ρ_s is the density of catalyst solid.

$$p_s=(p_{s,CO_2};\ p_{s,CH_4};\ p_{s,H_2};\ p_{s,CO};\ p_{s,H_2O})^T$$

The boundary conditions are as follows:

$$\frac{dp_{s,CO_2}}{d\xi}=\frac{dp_{s,CH_4}}{d\xi}=0 \qquad \text{at } \xi=0 \quad (28)$$

$$p_{s,CO_2}=p_{CO_2},\ p_{s,CH_4}=p_{CH_4} \qquad \text{at } \xi=1 \quad (29)$$

The profiles of other components are given as:

$$p_{s,CO}-p_{CO}=\left(\frac{D_{e,CO_2}}{D_{e,CO}}\right)(p_{CO_2}-p_{s,CO_2})-\left(\frac{D_{e,CH_4}}{D_{e,CO}}\right)(p_{s,CH_4}-p_{CH_4}) \quad (30)$$

$$p_{s,H_2O}-p_{H_2O}=\left(\frac{D_{e,CO_2}}{D_{e,H_2O}}\right)(p_{CO_2}-p_{s,CO_2})-\left(\frac{D_{e,CH_4}}{D_{e,H_2O}}\right)(p_{s,CH_4}-p_{CH_4}) \quad (31)$$

$$p_{s,H_2}-p_{H_2}=\left(\frac{D_{e,CO_2}}{D_{e,H_2}}\right)(p_{CO_2}-p_{s,CO_2})-\left(\frac{3D_{e,CH_4}}{D_{e,H_2}}\right)(p_{s,CH_4}-p_{CH_4}) \quad (32)$$

where D_{ei} is diffusivity of component A given as:

$$D_{ei}=\frac{\varepsilon_s}{\tau}\overline{D}_A \quad (33)$$

$$\frac{1}{D_A(r_i)}=\frac{1}{D_{mA}}+\frac{1}{D_{kA}(r_i)} \quad (34)$$

$$\overline{D}_A=\sum_i D_A(r_i)\cdot S(r_i) \quad (35)$$

$$S(r_i)=\frac{V_{g,i}}{\sum_i V_{g,i}}=\frac{V_{g,i}}{V_g} \quad (36)$$

where ε_s is the porosity of catalyst particle, τ the tortuosity factor, D_{mA} the molecular diffusivity of component A, D_{kA} the Knudsen diffusivity of component A, $S(r_i)$ the volume fraction of pores with radius r_i, V_g the volume of voids in a gram of catalyst and V_{gi} is the volume of void with pore radius r_i in a gram of catalyst.

The actual rates are accounted after computing the concentration profiles of components inside the catalyst particle as follows:

$$(r_j)_{obs}=\int_0^V r_j(p_s)\frac{dV}{V} \quad (37)$$

where V, P_s and ρ_s are the volume, pressure and density of catalyst pellet, respectively. The effectiveness factor is written as:

$$\eta_i=\frac{\int_0^V r_i(p_s)\rho_s\frac{dV}{V}}{r_i(p_s^s)\rho_s} \quad (38)$$

2-2. FT Reactor Model

Kinetic expressions of FT reactor with plug flow require a set of equations for all components, accounting for both solid and gas phase reactions in the catalyst bed and voids. For the gas phase, the mass and energy balance equations can be expressed as follows:

$$-\frac{f_{t0}}{A_c}\cdot\frac{dy_i}{dz}+a_v\cdot c_t\cdot k_{gi}\cdot(y_{is}-y_i)=0 \qquad i=1, 2, \ldots, N \quad (39)$$

$$-\frac{f_{t0}}{A_c}\cdot c_{pg}\cdot\frac{dT}{dz}+a_v\cdot h_f(T_s-T)+\frac{\pi D_i}{A_c}\cdot U_{shell}\cdot(T_{shell}-T)=0 \quad (40)$$

Here y_i gives the mole fraction for the gas phase, the cross section area of tube, a_v the specific surface area of catalyst pellet, c_t the total concentration, k_{gi} the mass transfer coefficient between gas and solid phase for component i, T the temperature of the gas phase, c_{pg} the specific heat of the gas at constant pressure, h_f the gas-catalyst heat transfer coefficient, D_i the tube inside diameter and U_{shell} is the Overall heat transfer coefficient between coolant and process streams. The boundary conditions applicable for this phase are:

$$\text{At } z=0;\ y_i=y_{i,in},\ T=T_{in} \tag{41}$$

In the solid phase, the mass and energy balance relations are represented by the following equations:

$$k_{gi}\cdot a_v\cdot c_t\cdot(y_i-y_{is})+\rho_B\cdot\eta\cdot r_i=0 \qquad i=1, 2, \ldots, N \tag{42}$$

$$a_v\cdot h_f\cdot(T-T_s)+\eta\cdot\rho_B\cdot\sum_{j=1}^{8} r_j\cdot(-\Delta H_{fj})=0 \tag{43}$$

where η and $\Delta H_{f,i}$ are the catalyst effectiveness factor and enthalpy of formation of component i, respectively. In previous work, Marvast et al. [15] developed a two-dimensional mathematical model of a Fischer-Tropsch reactor. One of the differences between the present study and Marvast et al. [15] is the feed of the FT process. On the other hand, in this work FT products changed with variation of SRM feed, but in Marvast, the FT products changed with variation of its feed.

The mass transfer coefficients between the gas and the catalytic phase were taken from Cussler [25]:

$$k_{gi}=1.17\mathrm{Re}^{-0.42}\mathrm{Sc}_i^{-0.67}u_g\times10^3 \tag{44}$$

$$\mathrm{Re}=\frac{2R_p u_g}{\mu} \tag{45}$$

$$s_{c_i}=\frac{\mu}{\rho\cdot D_{im}\cdot10^{-4}} \tag{46}$$

where R_p is the equivalent radius of the catalyst particle, u_g the gas velocity, μ the viscosity of the fluid. The diffusivity of components, D_{im}, defined in Eq. (46), can be written as [26]:

$$D_{im}=\frac{1-y_i}{\Sigma_{i\neq j}y_i D_{ij}} \tag{47}$$

$$D_{ij}=\frac{10^{-7}\cdot T^{3/2}\sqrt{\frac{1}{M_i}+\frac{1}{M_j}}}{P\left(\nu_{ci}^{3/2}+\nu_{cj}^{3/2}\right)^2} \tag{48}$$

D_{ij} is the binary diffusivity, M_i is the molecular weight of component i, and ν_{ci} is the critical volume of each component. These data are given in Table 5. The following correlation can be applied for calculation of the overall heat transfer coefficient between the shell (circulating boiling water) and tube (the bulk of the gas phase) sides U_{shell} that is used in Eq. (40):

$$\frac{1}{U_{shell}}=\frac{1}{h_i}+\frac{A_i\cdot\ln\frac{D_o}{D_i}}{2\pi LK_w}+\frac{A_i}{A_o}\cdot\frac{1}{h_o} \tag{49}$$

where A_i and A_o are the inner and outer area of each tube, respectively. D_o and D_i are the tube outside and inside diameter, respectively; L the Length of reactor, K_w the thermal conductivity of reactor wall and h_o is the heat transfer coefficient between coolant stream and reactor wall. The following equation is used to estimate the convection heat transfer coefficient, h_i, between the gas phase and the reactor wall [27]:

$$\frac{h_i}{c_p\rho\mu}\cdot\left(\frac{c_p\cdot\mu}{k}\right)^{2/3}=\frac{0.458}{\varepsilon_B}\cdot\left(\frac{\rho\cdot u\cdot d_p}{\mu}\right)^{-0.407} \tag{50}$$

where d_p and ε_B are the equivalent catalyst diameter and void fraction of the catalytic bed, respectively. c_p and k are the specific heat and thermal conductivity, respectively. The heat transfer coefficient of boiling water, h_o, in Eq. (49) can be calculated from the following equation [27]:

$$h_o=282.2p^{4/3}\cdot\Delta T^2 \qquad 0.7<P<14 \text{ MPa} \tag{51}$$

Table 5. Molecular weight and critical volume of the components

Component	M_i (g/mol)	ν_{ci} (m^3/mol)×10^6
C^{5+}	85.084	370
i-C_4H_{10}	58.123	262.7
n-C_4H_{10}	58.123	255
C_3H_8	44.096	200
C_2H_6	30.07	145.5
C_2H_4	28.054	129.1
CO_2	44.01	94.0
CO	28.01	18.0
H_2O	18.02	56.0
H_2	2.02	6.1
CH_4	16.04	99.0
N_2	28.01	18.5

3. Numerical Method

The reactor model was solved numerically by applying the finite difference approximation. The set of first-order ODEs of the model in the axial direction was applied for a system of coupled equations. This obtained ODEs system was solved using the Runge-Kutta method.

4. Assumptions

The present model has been made based on the following assumptions:

4-1. SRM Model

The main assumptions of the SRM model are: gas phase behaves as plug flow, the reactor is isothermal only in the radial direction, intraparticle temperature difference is negligible (isothermal solid phase), radial mass transfer is negligible, and a one-dimensional model is considered.

4-2. FT Model

The main assumptions of the FT model are: there are no radial concentration and temperature gradients, FT reactions take place at the catalyst surface, heat diffusion is negligible compared to convection, ideal gas law is valid, one-dimensional heterogeneous model is considered and the gas phase is considered to be plug flow.

SIMULATION RESULT AND DISCUSSION

It is well-known feature of the FT reaction that the product dis-

tribution cannot be closely controlled. Thus, one cannot obtain a hydrocarbon product in which the individual molecules all have exactly the same carbon atoms or even a product in some narrow range. However, the mathematical modelling and simulation in different operating conditions gives a clue to what is more important in formation of ethylene and other components. In principle, the effect of various parameters such as H_2O/CH_4 ratio, N_2/CH_4 ratio, GHSV, temperature and pressure in SRM reactor (The first reactor) was investigated on yield, selectivity as well as H_2 and CO conversion of FT reactor (the second reactor) output. Syngas is used to produce a variety of products in the FT reactor. Each product requires a specific ratio of H_2 to CO in the process feed gas to optimize production yields. In the present reactor configuration, outlet syngas stream of SRM is too rich in H_2 and is adjusted by using membranes to selectively strip out the excess H_2. The H_2 : CO ratio is optimized effectively using membrane systems and enters the FT reactor.

1. Verification of Reactors Model

The verification of each of model is necessary before it can be used for simulation.

1-1. Steam Reforming of Methane

The verification of the model presented in this work is compared to the experimental results of the industrial SRM reactor reported by Xu et al. [17] in terms of methane and steam conversion, temperature, pressure and component partial pressure. As can be seen in Table 6, methane and H_2O conversion as well as temperature and pressure obtained from modelling of reactor show good agreement with the experimental data. The partial pressures obtained were also in good agreement with those obtained from pilot plant testing. The small deviation between these amounts is due to considered assumptions in model as well as mass and heat resistances.

1-2. Fischer-Tropsch

The model was validated by comparing the results with experimental data of FT pilot plant [15] in the same temperature, inlet pressure and feed molar ratio. The proposed model was validated against pilot plant data of RIPI listed in Table 7. As can be clearly seen, good agreement exists between calculated values and experimental data in terms of selectivity and conversion.

2. Sensitivity Analysis

2-1. Effect of H_2O/CH_4 Ratio in SRM Feed

Fig. 2 depicts the variation of the CH_4 and H_2O conversion and

Table 6. Comparison between model results with experimental data for OCM

Parameter	Pilot plant data	Calculated	Error (%)
X_{CH_4} (%)	58	60.3	3.96%
X_{CO_2} (%)	33	31.5	4.5%
P_t	25.7	24.77	3.6%
T	1023	1070	4.6%
Partial pressure at Z=4 from the inlet			
CO	0.27	0.2849	5.5%
H_2	6.07	6.05	6.4%
CH_4	4	4.09	2.25%
CO_2	1.62	1.44	11.11%
H_2O	15.75	15.94	1.2%

Table 7. Comparison of simulated and pilot plant data for FT synthesis

Parameter	Pilot plant data	Calculated	Error (%)
X_{CO} (%)	92.83	94.5	1.8%
X_{H_2} (%)	77.94	77.19	0.96%
C_5 selectivity	42.55	45.64	7.3%
CO_2 selectivity	339.07	317.32	6.4%
CH_4 selectivity	44.15	44.65	1.1%
H_2O selectivity	120.67	115.19	4.5%
C_2H_4 selectivity	3.95	3.52	1.1%
C_2H_6 selectivity	11.78	13.93	18.25%
n-C_4 selectivity	11.07	9.65	12.82%
i-C_4 selectivity	14.45	12.23	15.36%
C_3H_8 selectivity	9.33	6.42	31.19%

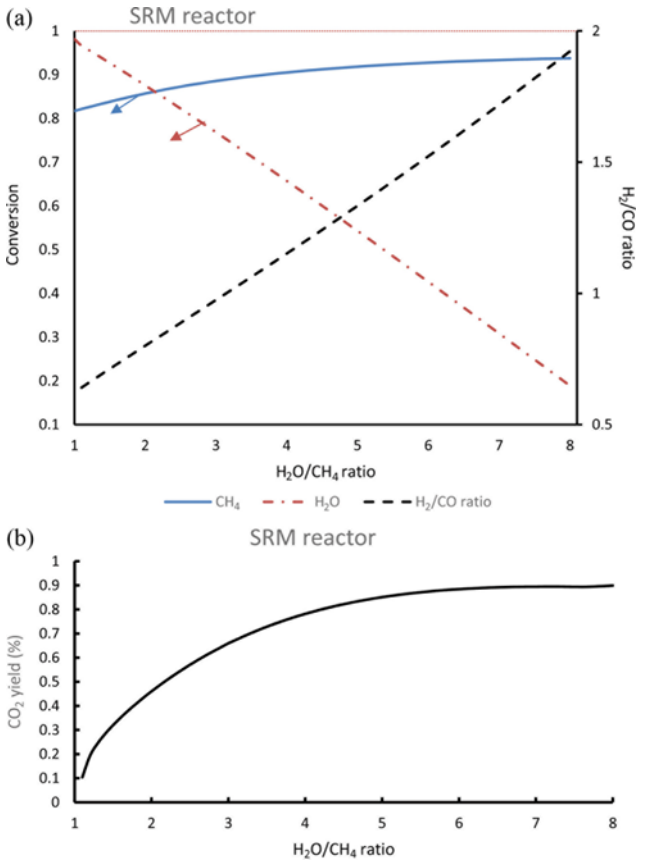

Fig. 2. Variation of (a) H_2O and CH_4 conversions and H_2/CO ratio (b) CO_2 yield in SRM reactor as a function of H_2O/CH_4 ratio (CO_2/CH_4=0.056, H_2/CH_4=0.122, N_2/CH_4=0.162, T=793.15 K, P=29 bar).

H_2/CO ratio in SRM reactor versus H_2O/CH_4 ratio in feed gas while other parameters are constant. As shown, an increase in H_2O/CH_4 ratio enhances CH_4 conversion; that is due to increase of reaction rate with adding further H_2O to SRM feed. On the other hand, the steam makes reforming reactions react with excess H_2O. Fig. 2 also shows that the H_2O conversion decreases with H_2O/CH_4 ratio because of increasing its amount in feed. H_2/CO ratio increases

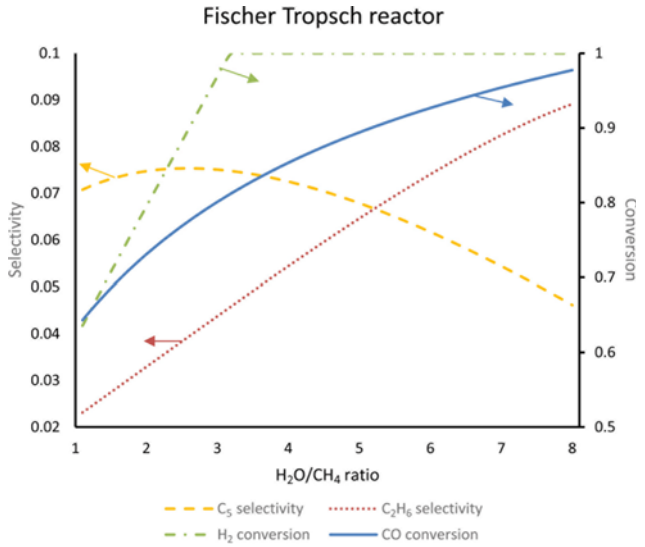

Fig. 3. Effect of H_2O/CH_4 ratio in SRM reactor feed on H_2 and CO conversions and C_5 and C_2H_4 selectivity in conventional FT reactor (CO_2/CH_4=0.056, H_2/CH_4=0.122, N_2/CH_4=0.162, T=793.15 K, P=29 bar).

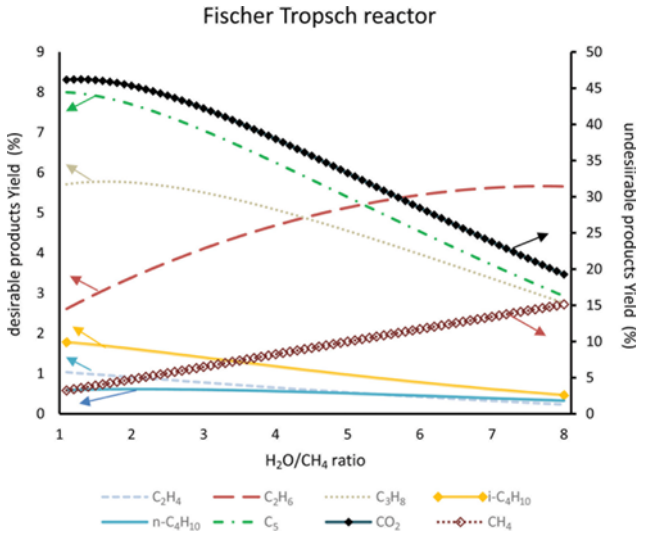

Fig. 4. Effect of H_2O/CH_4 ratio in SRM reactor feed on yield of desired products and also yield of CO_2 and CH_4 as undesired products in FT reactor (CO_2/CH_4=0.056, H_2/CH_4=0.122, N_2/CH_4=0.162, T=793.15 K, P=29 bar).

from 0.65 to 2 with more H_2O/CH_4 in feed of SRM reactor (Fig. 2). Increase of steam flow rate in feed resulted in consumption of carbon monoxide because it is consumed by water gas shift reactions. When methane is fed to the SRM unit, it is converted to CO_2 as well as other products. CO_2 content can affect FT reaction. Therefore, yield of CO_2 is shown in Fig. 2(b) as H_2O/CH_4 varies in SRM reactor.

The influence of H_2O/CH_4 ratio in SRM feed on the CO and H_2 conversions and selectivity of gasoline and ethane in FT synthesis is demonstrated in Fig. 3. Fig. 3 shows that an increase in the steam to methane ratio feed (H_2O/CH_4=1-8) causes increase of synthesis gas conversions and the value of H_2 conversion is more than CO. Moreover, at higher ratios, hydrogen conversion is complete, while carbon monoxide also reacts in the water gas shift reaction. As shown, higher H_2O/CH_4 ratio causes lower C_5 and higher C_2H_6 selectivity. These diagram trends are due to the differences in rates of these components. Selectivity of C_5 is first increased and then decreased because the amount of CO in FT reactor is increased. This effect also relates to H_2/CO ratio in SRM reactor. With increasing H_2O/CH_4 ratio more H_2 and CO can be produced, but in this process H_2 amount which is achieved is more than CO, and as a result, C_5 selectivity increases. In FT reactions the produced H_2 in the previous SRM process is consumed more than CO; as a result, gasoline rate is varied and its selectivity is reduced. Ethane selectivity is increased because of hydrogen variation effect on selectivity of this component.

Selectivity and yield of each component is defined as:

$$\text{Selectivity} = \frac{\text{Moles of C atom in FT products}}{\text{Moles of methane consumed in SRM feed}}$$

$$\text{Yield} = \frac{\text{Moles of C atom in FT products}}{\text{Moles of inlet methane in SRM}}$$

Fig. 4 shows the effect of SRM reactor H_2O/CH_4 feed ratio on the yield of products in FT reactor. The results show that at higher H_2O/CH_4 ratio (and low CO in feed), lower C_2-C_5 and CO_2 yield is obtained except for C_2H_6 and CH_4. In this situation lower amount of CO is produced in SRM, and as C_2H_6 rate depends differently on CO, the production of C_2H_6 is more. As shown in Table 4, the partial pressure exponent of carbon monoxide in ethane rate is negative. Thus, the ratio of H_2/CO in the reaction mixture has a pronounced effect on yield as well as on reaction rate. At a ratio of 2 : 1 the conversion reached 95% and ethane production was almost more than others; at a 0.65 : 1 ratio the conversion was only 65% but products were obtained from methane to gasoline. Moreover, the yields of two unfavorable products, methane and carbon dioxide, are shown in this figure. The figure shows that with increase of H_2O/CH_4 ratio, CO_2 yield is decreased, whereas yield of CH_4 is increased. This is most probably because CO is decreased in high H_2O/CH_4 ratio and quantity of carbon dioxide produced from water gas shift reaction decreases as well as increase in methane yield. Krishnamoorthy et al. [28] investigated the pathways for CO_2 formation in FT and found that primary pathways for the removal of adsorb oxygen formed in CO dissociation steps include reactions with adsorbed hydrogen to form H_2O and with adsorbed CO to form CO_2. The H_2O selectivity for these pathways is much higher than that predicted from water gas shift reaction equilibrium; therefore, readsorption of H_2O followed by its subsequent reaction with CO derived intermediate leads to the net formation of CO_2 with increasing reactor residence time [28]. Thus the addition of CO_2 could lead to the minimization of CO_2 formation during FT and to the preferential removal of oxygen as H_2O. This, in turn, leads to lower average H_2/CO ratios throughout the catalyst bed and to higher olefin content and C_5 selectivity.

2-2. Effect of N_2/CH_4 Ratio in SRM Feed

Inert gas acts as diluent in the SRM process. The presence of nitrogen as inert gas in the SRM feed was simulated for its effect on yield, conversion and selectivity of FT products. It is clearly obvi-

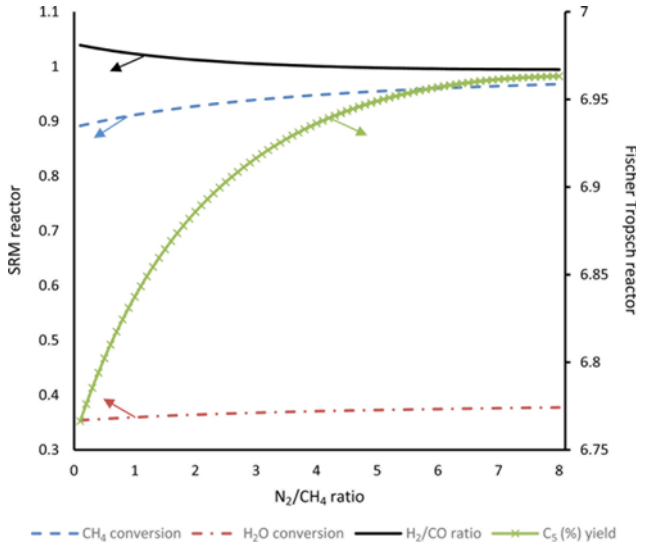

Fig. 5. Variation of H_2/CO ratio, H_2O and CH_4 conversions in SRM reactor and C_5 yield in FT reactor as a function of N_2/CH_4 ratio in SRM feed (CO_2/CH_4=0.056, H_2/CH_4=0.122, H_2O/CH_4=3.358, T=793.15 K, P=29 bar).

ous that remarkable effect is achieved in presence of N_2. As shown in Fig. 5 a decrease in hydrogen to carbon monoxide ratio is observed with increasing N_2/CH_4 ratio in feed because diluent concentration decreases rate of hydrogen and carbon monoxide formation. However, amount of CO produced is greater than H_2 because carbon monoxide is produced in all reactions whereas hydrogen is consumed in reverse water gas shift reaction. Moreover, with increasing diluent concentration, H_2O and CH_4 conversions increased. These variations are due to increasing rate of reactions. The yield of gasoline is also shown in this figure. As shown, the yield of C_5 increased with increasing of N_2 inert gas. Due to the dilution effect of nitrogen, H_2/CO ratio moves to optimum value (=0.8) reported by Rahimpour et al. [29], which in this ratio, FT reactions have their best performance.

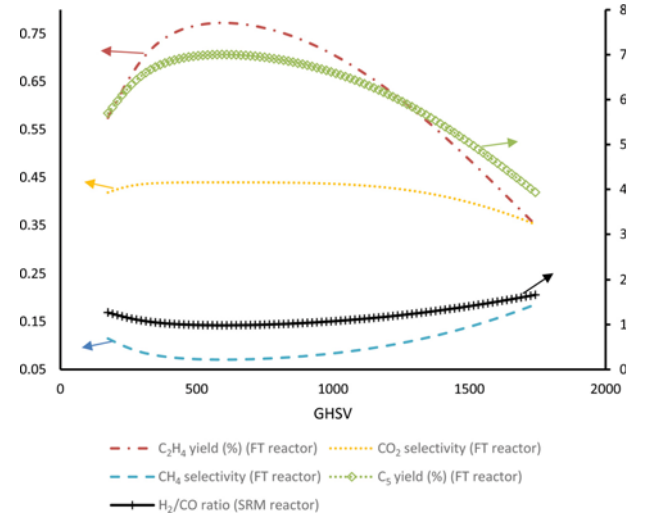

Fig. 6. Variation of H_2/CO ratio in SRM reactor, C_2H_4 and C_5 yields in FT reactor, CO_2 and CH_4 selectivity in FT reactor as a function of GHSV in SRM reactor (N_2/CH_4=0.162, CO_2/CH_4=0.056, H_2/CH_4=0.122, H_2O/CH_4=3.358, T=793.15 K, P=29 bar).

2-3. Effect of GHSV in SRM Reactor

GHSV is gas hourly space velocity. The GHSV is the ratio of gas flow in standard condition to the volume of the bed (only active phase, catalyst). This operating parameter has a significant effect on reactions conversion and products yield. Results of simulation for GHSV effects are presented in Fig. 6. Clearly, GHSV has a significant effect on the products. As indicated by Fig. 6, H_2/CO ratio decreases with GHSV until it reaches a minimum ratio of about 0.95 and then increases. Increasing the amount of GHSV causes a reduction of contact time, and so decreases the amounts of CO and H_2 in SRM. However, in lower amounts of GHSV more hydrogen is produced; therefore, water gas shift reaction drives in the reverse direction for producing CO. As a result, H_2/CO ratio decreases at first. When flow rate and GHSV increase, the amount of products is less than previous cases and greater amount of steam remains. The increasing in amount of steam affects the water gas shift reaction and produces H_2 and we will have higher H_2/CO in SRM reactor. Fig. 6 also depicts the effect of GHSV on the C_5 and C_2H_4 yields. Increase of the yield of C_2H_4 and C_5 was due to decrease of H_2/CO ratio to the optimum value. The variation of CH_4 and CO_2 selectivity as undesired products at different GHSV is shown in Fig. 6. It is obvious that the steam amount is drastically increased due to increasing of GHSV and as a result reacts with carbon monoxide and produces CO_2. However, with increasing CO_2, reverse of WGS reaction occurs and the CO_2 amount decreases. Trend of CH_4 diagram is due to the fact that the rate equation of methane differently depends on H_2 and CO.

2-4. Component Mole Flow and Conversion in Reactors

Fig. 7 shows the conversions of CH_4 and H_2O at 793 K along the SRM reactor. As shown, conversion of methane is more than steam. Since, CH_4 is consumed in all of SRM reactions while steam is produced in some of reactions. Molar flow of components in the two reactors length is indicated by Fig. 8(a), (b). As shown in Fig.

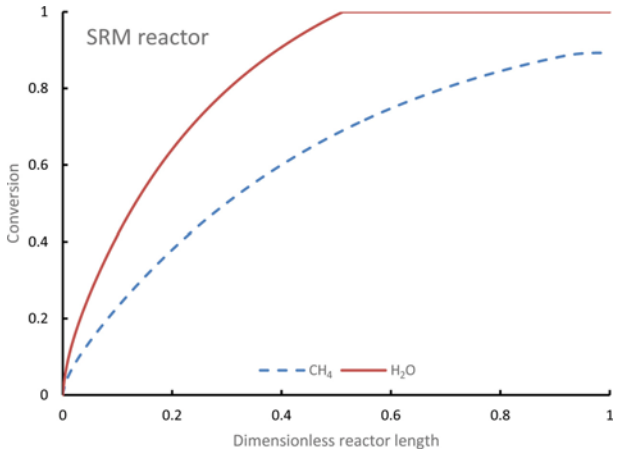

Fig. 7. Variation of CH_4 and H_2O conversion in two consecutive reactors of SRM and FT (N_2/CH_4=0.162, CO_2/CH_4=0.056, H_2/CH_4=0.122, H_2O/CH_4=3.358, T=793.15 K, P=29 bar).

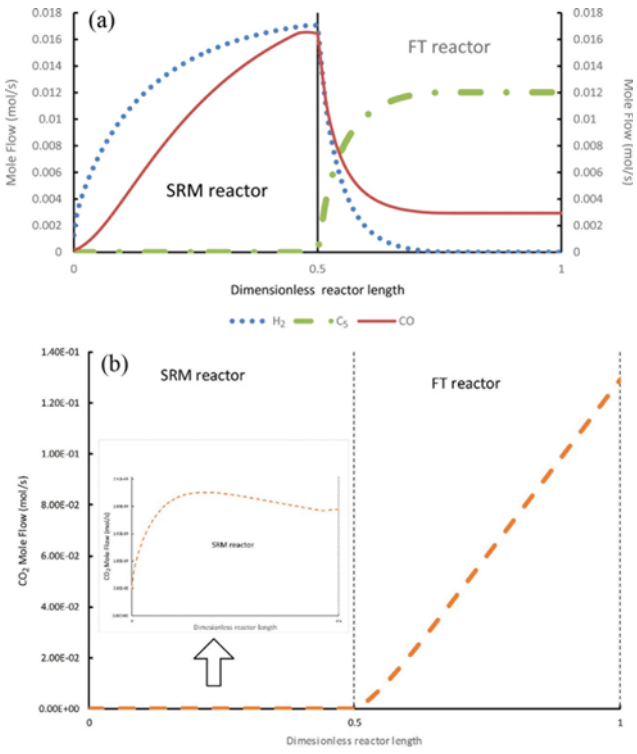

Fig. 8. Variation of (a) H_2, CO and C_5 (b) CO_2 (c) C_2H_6, C_3H_8, i-C_4H_{10}, n-C_4H_{10} and C_5 mole flow in two consecutive reactors of SRM and FT (N_2/CH_4=0.162, CO_2/CH_4=0.056, H_2/CH_4=0.122, H_2O/CH_4=3.358, T=793.15 K, P=29 bar).

8(a), H_2 and CO produced in SRM reactor are consumed in the FT process. The diagram indicates that fresh feed's hydrogen is completely consumed in the middle of FT reactor and the water gas shift reaction still continues. The small amount of hydrogen produced in this reaction is further converted to hydrocarbons. Fig. 7 also indicates the gasoline mole flow produced in the FT reactor. As shown, gasoline is produced in the FT reactor with high rate at first and then the production rate decreases. This variation is because all of hydrogen feed is consumed and as a result not carry out the FT reactions. Fig. 8(b) shows the carbon dioxide mole flow in the two reactors length. As can be seen, CO_2 is produced in both SRM and FT reactors, although its production is much more in FT reactor. Molar flow profile of other components along the FT reactor is shown in Fig. 9. As can be seen, the variations in components mole flow is only significant at dimensionless lengths lower than 0.25, and afterward the components change more slowly. In Fig. 9 the change in CO conversion is small after complete consumption of H_2.

2-5. Pressure and GHSV in SRM Reactor

Fig. 10(a) indicates the influence of both inlet pressure and GHSV in SRM on gasoline selectivity. Results show that ethylene selectivity decreases with increase in the SRM pressure. With GHSV, selectivity of gasoline initially increases and then attains lower values. This behavior with increasing pressure can be justified by Le Chatelier's principle. According to Le Chatelier's principle, by increasing the reactor pressure the reaction moves to the side with lower number of moles to compensate the effect of increasing pressure.

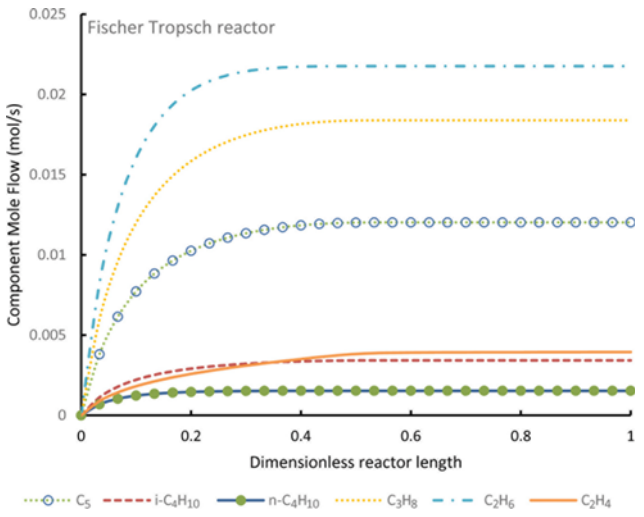

Fig. 9. Variation of C_2H_6, C_2H_4, C_3H_8, i-C_4H_{10}, n-C_4H_{10} and C_5 mole flow in FT reactor (N_2/CH_4=0.162, CO_2/CH_4=0.056, H_2/CH_4=0.122, H_2O/CH_4=3.358, T=793.15 K, P=29 bar).

In other words, an increase in the SRM inlet pressure decreases the hydrogen product and as a result decreases the C_5 selectivity. As the results indicate, the effect on a particular range of products may be quite small for pressure changes of several bar. Research also shows that beyond a certain point the yield of all products begins to fall off with further increase of pressure. This has been attributed to carbonyl formation, but may also be due to the blocking of the catalyst surface [30].

Fig. 10(b) indicates variation of gasoline yield versus both temperature and steam to methane ratio. This 3-D diagram indicates that C_5 yield is increased with increasing temperature. The influence of temperature and pressure on the course of the reaction is straightforward. Increasing the temperature increases the rate of reaction, but decreases the chain length of the products, whereas increasing total pressure increases both the extent of conversion and the chain length of the products.

2-6. Temperature Profiles

Fig. 11 shows the temperature profile of FT and SRM processes along the reactors dimensionless length. SRM reactions are endothermic; however, due to high temperature of furnace and high heat transfer of the wall with reactions zone, the temperature in SRM reactor increases. For FT there is a peak temperature close to the inlet of the reactor and then temperature reduction is observed. This peak is due to the exothermic reactions of FT.

CONCLUSION

The significance of two consecutive reactors is that it provides the choice of producing gasoline and other hydrocarbons from methane. Since SRM contains good amounts of CO and H_2, carbon monoxide hydrogenation using FT is promising. The proposed configuration shows complete conversion of hydrogen in second reactor, although a small amount of carbon monoxide remains in it. More detailed simulation showed that C_5 selectivity and yield is increased at higher H_2O/CH_4 ratio because H_2/CO ratio is high.

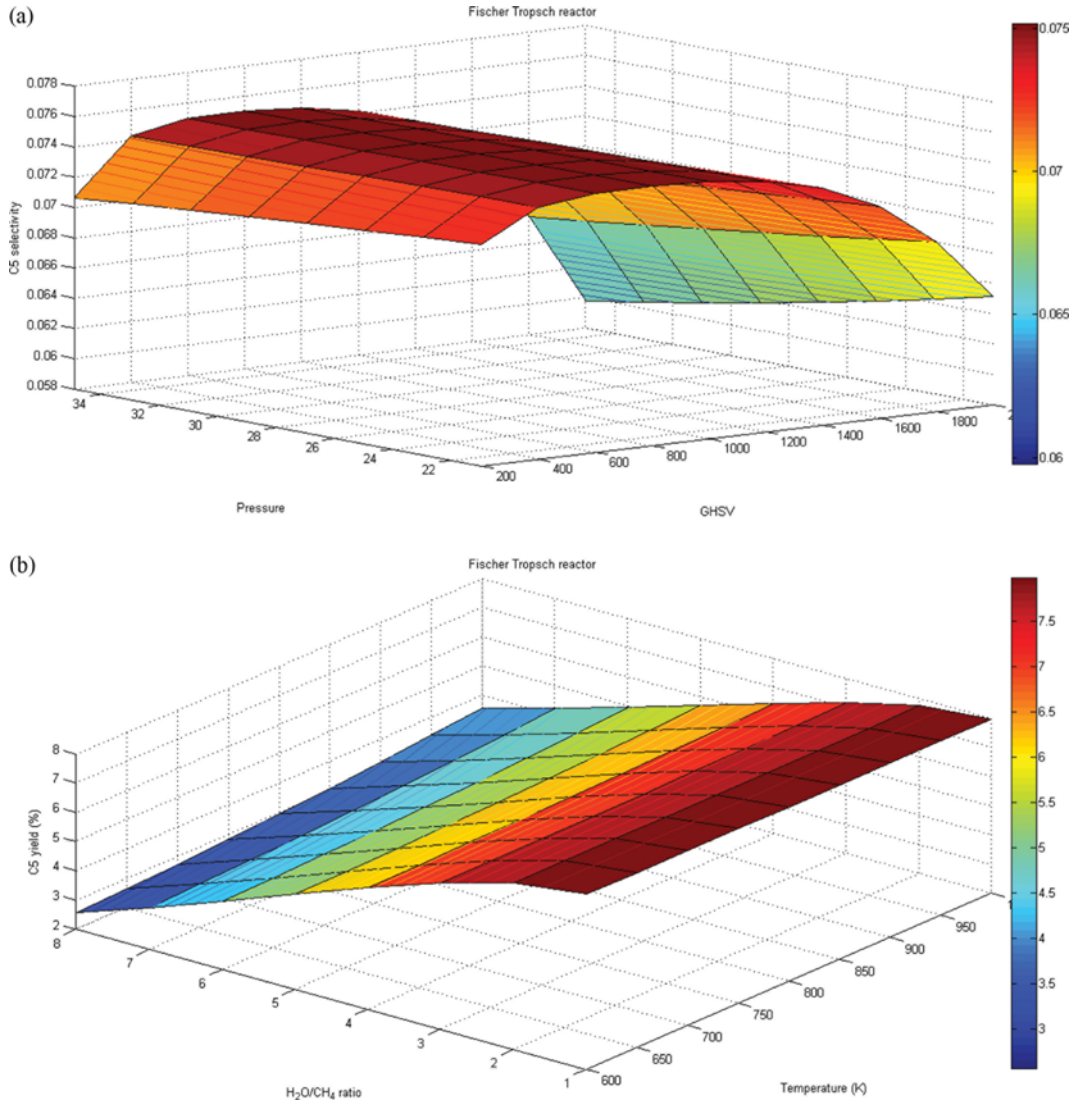

Fig. 10. Three-dimensional profiles of (a) gasoline selectivity in the exit of FT in terms of pressure and GHSV of SRM reactor (b) gasoline yield in the exit of FT in terms of H_2O/CH_4 ratio and temperature of SRM reactor.

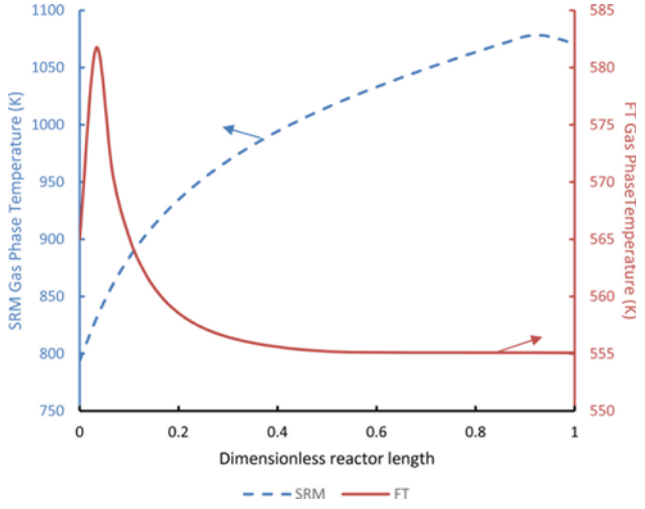

Fig. 11. Temperature profile in SRM and FT reactors.

SYMBOLS

A_c : cross section area of tube [m^2]
A_i : inner area of each tube [m^2]
A_s : lateral area of each tube [m^2]
A_{shell} : cross section area of shell [m^2]
a_v : specific surface area of catalyst pellet [$m^2 \cdot m^{-3}$]
a_m : surface area of the catalyst pellet per kg cat [m^2/kg cat]
c_i : concentration of component I in gas phase [kmol/m^3]
c_p : specific heat [kJ·mol^{-1}·K]
c_{pg} : specific heat of the gas at constant pressure [J·mol^{-1}·k^{-1}]
c_{ph} : specific heat of the hydrogen at constant pressure [J·mol^{-1}·k^{-1}]
c_{Ps} : specific heat of the catalyst at constant pressure [J·mol^{-1}·k^{-1}]
$c_{s,i}$: concentration of component I inside catalyst pellet [kmol/m^3]
c_t : total concentration [mol·m^{-3}]

D_A : effective diffusivity of component A [m^2/h]
D_{eA} : diffusivity of component A [m^2/h]
D_{mA} : molecular diffusivity of component A [m^2/h]
D_{KA} : knudsen diffusivity of component A [m^2/h]
D_i : tube inside diameter [m]
D_o : tube outside diameter [m]
D_{ij} : binary diffusion coefficient of component i in j [$m^2 \cdot s^{-1}$]
D_m^i : diffusion coefficient of component i in the mixture [$m^2 \cdot s^{-1}$]
D_{ro} : reaction outside diameter [m]
d_p : diameter of the catalyst pellet [m]
d_{pe} : external diameter of the catalyst ring [m]
d_{pi} : inner diameter of the catalyst [m]
d_{le} : external diameter of the reactor tube [m]
d_{li} : inner diameter of the reactor tube [m]
$F^0_{CH_4}$: molar flow rate of CH_4 in the feed [kmol/h]
$F^0_{CO_2}$: molar flow rate of CO_2 in the feed [kmol/h]
f_{t0} : total molar rate in tube at entrance of reactor [$mol \cdot s^{-1}$]
f : fraction factor in the momentum equation
f(r) : fraction of pores with radius r
g : acceleration of gravity [m/h^2]
H : height of the catalyst ring [m]
h_f : gas-catalyst heat transfer coefficient [$W \cdot m^{-2} \cdot K^{-1}$]
h_i : heat transfer coefficient between fluid phase and reactor wall [$W \cdot m^{-2} \cdot K^{-1}$]
h_o : heat transfer coefficient between coolant stream and reactor wall [$W \cdot m^{-2} \cdot K^{-1}$]
K : conductivity of fluid phase [$W \cdot m^{-1} \cdot K^{-1}$]
K_i : equilibrium constant of reactions I, II, III [bar^2, _, bar^2]
K_j : adsorption constant for component j
j=CO, H_2, CH_4 [bar^{-1}]
j=H_2O
k_i : rate coefficient of reaction i
i=I, III [$kmol \cdot bar^{-0.5}$/(kg cat·h)]
i=II [kmol/(kg cat·h·bar)]
l : thickness of the active part on each side of the catalyst ring [m]
K_w : thermal conductivity of reactor wall [$W \cdot m^{-1} \cdot K^{-1}$]
k_{gi} : mass transfer coefficient between gas and solid phase for component i [$m \cdot s^{-1}$]
L : length of reactor [m]
M_i : molecular weight of component I [$g \cdot mol^{-1}$]
N : number of components [-]
P_t : total pressure [bar]
P_i : partial pressure of component i [bar]
P_a : atmospheric pressure [bar]
R : gas constant [kJ/(kmol·K)]
Re : Reynolds number
R_p : equivalent radius of the catalyst particle [m]
r_i : reaction rate of component i [$mol \cdot kg^{-1} \cdot s$]
$r_{g,i}$: rate of formation of gas-phase reaction i [$mol \cdot kg^{-1} \cdot s$]
r_{CH_4} : total rate of disappearance of CH_4 in steam reforming [kmol CH_4/(kg cat·h)]
r'_{CH_4} : rate of formation of CH_4 in reverse of water gas shift [kmol CH_4/(kg cat·h)]
r_{CO_2} : rate of conversion of CH_4 into CO_2 in steam reforming [kmol CH_4/(kg cat·h)]
r'_{CO_2} : rate of disappearance of CO_2 in reverse of water gas shift [kmol CO_2/(kg cat·h)]
r : pore radius [m]
S : volume fraction of pores with radius (r_i<r<r_{i+1})
T : process gas Temperature [K]
T_t : internal tube skin temperature [K]
T_s : external temperature [K]
T_{shell} : temperature of coolant stream, in fixed bed reactor [K]
T_w : external tube skin temperature [K]
U : overall heat transfer coefficient [$W \cdot m^{-2} \cdot K$]
U_{shell} : overall heat transfer coefficient between coolant and process streams [$W \cdot m^{-2} \cdot K^{-1}$]
u_s : superficial velocity [$m_f^3/(m_r^2 \cdot h)$]
V : volume of catalyst pellet [m^3]
V_g : volume of voids in a gram of catalyst [mL/g_{cat}]
V_{gi} : volume of void with pore radius r_i<r<r_{i+1} in a gram of catalyst [mL/g_{cat}]
V(i) : exponential of reaction affinity
W : amount of catalyst in the reactor [kg]
x : distance from surface of catalyst onwards
x_{CH_4} : conversion of CH_4
x_{CO_2} : conversion of CH_4 into CO_2
x'_{CH_4} : conversion of CO_2 into CH_4 when CO_2 and H_2 are fed
x'_{CO_2} : total conversion of CO_2 in reverse of water gas shift
y_i : mole fraction of component i in the fluid phase [$mol \cdot mol^{-1}$]
y_{is} : mole fraction of component i in the solid phase [$mol \cdot mol^{-1}$]
Z : axial reactor coordinate [m]

Greek Letters

α_i : convective heat transfer coefficient in packed bed [kJ/(m^2·H·K)]
η : catalyst effectiveness factor
η_{CH_4} : effectiveness factor for methane disappearance
η_{CO_2} : effectiveness factor for CO_2 formation
η_i : effectiveness factor of reaction i, i=I, II, III
η'_1, η'_2, η'_3 : effectiveness factor of the reverse of reactions I, II, III
ε_s : porosity of catalyst particle [m^3_{void}/m^3_{cat}]
ε_B : void fraction of catalytic bed [-]
λ_g : thermal conductivity of the process gas [kJ/(m·h·K)]
λ_{si} : thermal conductivity of the tube metal [kJ/(m·h·K)]
ρ_b : density of catalyst in the bed [kg cat·m^{-3}]
ρ_g : density of system gas [kgm^{-3}]
ρ_s : density of catalyst solid [kg cat·m^{-3}]
ξ : radial position in particle
ζ : CO_2/CH_4 molar feed ratio [$kmol_{CO_2}/kmol_{CH_4}$]
τ : tortuosity factor
μ : viscosity of the fluid [kg/(m·s)]
$\Delta H_{f,i}$: enthalpy of formation of component I [$J \cdot mol^{-1}$]
ΔH_i : enthalpy change of reaction I [kJ/kmol]
Ω : cross section of the reactor [m^2]
ν_j : stoichiometric coefficient of component j in reaction i

REFERENCES

1. C. H. Bartholomew and R. J. Farrauto, *In Fundamentals of industrial catalytic processes*, Wiley, Hoboken, New Jersey, USA, Chap-

ter 6 (2006).
2. M. A. Soliman, S. S. E. H. El-Nashaie, A. S. Al-Ubaid and A. Adris, *Chem. Eng. Sci.*, **43**, 1801 (1988).
3. A. M. Adris, C. J. Lim and J. R. Grace, *Chem. Eng. Sci.*, **52**, 1609 (1997).
4. M. De Falco, L. Di Paola, L. Marrelli and P. Nardella, *Chem. Eng. J.*, **128**, 115 (2007).
5. P. Sadooghi and R. Rauch, *J. Nat. Gas. Sci. Eng.*, **11**, 46 (2013).
6. X. Wu, Ch. Wu and S. Wu, *Chem. Eng. Res. Des.*, **96**, 150 (2015).
7. W. D. Deckwer, Y. Serpemen, M. Ralek and B. Schmidt, *Ind. Eng. Chem. Proc. Des. Dev.*, **21**, 231 (1982).
8. J. R. Turner and P. L. Mills, *Chem. Eng. Sci.*, **45**, 2317 (1990).
9. H. S. Song, D. Ramkrishna, S. Trinh and H. Wright, *Korean J. Chem. Eng.*, **21**, 308 (2004).
10. J. Wu, H. Zhang, W. E. I. Y. O. N. G. Ying and D. Fang, *Chem. Eng. Technol.*, **33**, 1083 (2010).
11. N. Park, J. R. Kim, Y. Yoo, J. Lee and M. J. Park, *Fuel*, **122**, 229 (2014).
12. Y. H. Kim, K. W. Jun, H. Joo, C. Han and I. K. Song, *Chem. Eng. J.*, **155**, 427 (2009).
13. A. K. Avci, D. L. Trimm and Z. İlsen Önsan, *Chem. Eng. Sci.*, **56**, 641 (2001).
14. M. Johns, P. Collier, M. S. Spencer, T. Alderson and G. J. Hutchings, *Catal. Let.*, **90**, 187 (2003).
15. M. A. Marvast, M. Sohrabi, S. Zarrinpashne and G. Baghmisheh, *Chem. Eng Technol.*, **28**, 78 (2005).
16. A. N. Pour, S. M. K. Shahri, Y. Zamani, M. Irani and S. Tehrani, *J. Nat. Gas. Chem.*, **17**, 242 (2008).
17. J. Xu and G. F. Froment, *AIChE J.*, **35**, 88 (1989).
18. M. M. Montazer-Rahmati and M. Bargah-Soleimani, *Can. J. Chem. Eng.*, **79**, 800 (2001).
19. H. Brauer, *Chem. Ing. Technol.*, **29**, 785 (1957).
20. W. Reichelt and E. Blaβ, *Chem. Ing. Technol.*, **43**, 949 (1971).
21. S. Ergun, *Chem. Eng. Prog.*, **48**, 89 (1952).
22. A. P. De Wasch and G. F. Froment, *Chem. Eng. Sci.*, **27**, 567 (1972).
23. G. F. Froment and K. B. Bischoff, *Chemical Reactor Analysis and Design*, John Wiley, New York (1979).
24. D. Kunii and J. M. Smith, *AIChE J.*, **6**, 71 (1960).
25. E. L. Cussler, Diffusion, Mass Transfer in Fluid Systems, Cambridge: Cam. Univ. Press, 525: ll (1984).
26. C. R. Wilke, *Chem. Eng. Prog.*, **45**, 218 (1949).
27. M. Panahi, MSc thesis, Sharif University of Technology, Tehran, Iran (2005).
28. S. Krishnamoorthy, A. Li and E. Iglesia, *Catal. Let.*, **80**, 77 (2002).
29. M. R. Rahimpour and H. Elekaei, *Fuel. Proc. Technol.*, **90**, 747 (2009).
30. R. C. Everson, E. T. Woodburn and A. R. M. Kirk, *J. Catal.*, **53**, 186 (1978).